Rapid monitoring of cleaning efficiency of fouled hollow fiber membrane module via non-invasive NMR diffraction technique

Yan, Bin; Vogt, Sarah J.; Blankert, Bastiaan; Vrouwenvelder, Johannes; Johns, Michael L.; Fridjonsson, Einar O.

Important note
To cite this publication, please use the final published version (if applicable).
Please check the document version above.

Rapid monitoring of cleaning efficiency of fouled hollow fiber membrane module via non-invasive NMR diffraction technique

Bin Yan [a], Sarah J. Vogt [a], Bastiaan Blankert [b], Johannes Vrouwenvelder [b,c], Michael L. Johns [a], Einar O. Fridjonsson [a,*]

[a] Department of Chemical Engineering, The University of Western Australia, Crawley, WA 6009, Australia
[b] Biological and Environmental Sciences and Engineering Division, Water Desalination and Reuse Center, King Abdullah University of Science and Technology, Thuwal 23955-6900, Saudi Arabia
[c] Department of Biotechnology, Faculty of Applied Sciences, Delft University of Technology, Van der Maasweg 9, 2629 HZ Delft, The Netherlands

ARTICLE INFO

ABSTRACT

Early fouling warning is important for the economical operation of membrane separation systems. In parallel multi-channel flow systems, flow re-distribution between channels due to fouling is often associated with maloperation. In the current research we use low magnetic field NMR to monitor multi-fiber hollow fiber membrane modules undergoing a fouling-cleaning cycle and show that rapid detection of fouling is possible by detecting the loss of signal coherence associated with flow re-distribution within the 401 hollow fiber membrane module. This effect is demonstrated to be both reproducible, and reversible via membrane cleaning. The results demonstrate a strong correlation between the coherence signal magnitude and the number of fibers fouled. This may be used in practice for high sensitivity early warning, and to monitor the efficiency of cleaning. This approach may also be particularly useful in the case of detecting residual fouling after cleaning, evidenced in this research by significant flow re-distribution between the before fouling and after cleaning signal coherence.

1. Introduction:

Early warning of fouling is important for the efficient operation of membrane separation technologies by optimising cleaning chemical use and downtime (Saad, 2004; Vrouwenvelder et al., 2006; Vrouwenvelder et al., 2011). Li et al. (Li et al., 2017) in 2018 reviewed technologies for the in-situ monitoring of fouling in hollow fiber membrane processes, including magnetic resonance imaging (MRI), concluding that it would be of great significance to broaden the application of these technologies to industrial processes so as to improve the design of membrane modules. The same year Sim et al. (Sim et al., 2018) reviewing monitoring techniques for reverse osmosis found that only ultrasonic time-domain reflectometry (UTDR) and nuclear magnetic resonance (NMR) had been shown to be able to monitor membrane performance in spiral wound membranes (SWMs) non-invasively in real time. To expand upon these current capabilities of NMR real time monitoring of fouling in hollow fiber membrane modules, in this work, we present a novel technique of monitoring NMR signal diffraction phenomena, caused by the breakdown of flow symmetry due to fouling.

In chemical engineering classical diffraction phenomena based on wave scattering are often used for the structural characterisation of membranes and catalysts (Marchesini et al., 2003; Tanner, 2013; Grunwaldt and Schroer, 2010; Albers and Parker, 2021; Gebel and Diat, 2005). Barrall *et al.* (Barrall et al., 1992), building on the work of Mansfield and Grannell (Mansfield and Grannell, 1973; Mansfield and Grannell, 1975), showed that it was possible to characterise small scale sample heterogeneities present in NMR diffraction data using NMR Patterson functions, which are analogous to their counterpart in x-ray diffraction (Warren, 1990). The benefit of this approach is that the number of acquisition points, and therefore acquisition time, required reduces to approximately the number of features in the sample. This has significant benefits towards increasing the temporal resolution of monitoring techniques. This type of NMR diffraction analysis has previously been used to probe sample structure using direct imaging of the sample spatial spin distribution (Barrall et al., 1992) as is done in the current work, and sampling of the system structure by spin molecular dynamics (Callaghan et al., 1991; Callaghan et al., 1999; Seymour and Callaghan, 1997; Song et al., 2000; Shemesh, 2020), for example to

---

* Corresponding author.
 E-mail address: einar.fridjonsson@uwa.edu.au (E.O. Fridjonsson).

measure the surface to volume ratio of porous media (Sen et al., 1995).

Modern MRI techniques (e.g. compressed sensing (Lustig et al., 2007) combined with Rapid Imaging with Refocused Echoes (RARE) (Schuhmann et al., 2018) allow MRI acquisition on rapid time scales (e. g. < 1 s) but their practical application is often curtailed at low magnetic fields due to low signal-to-noise (SNR). As SNR $\propto \omega_0^{7/4}$ (Hoult and Richards, 1976) where ω_0 is the Larmor frequency. The compromise between SNR and temporal resolution must therefore be carefully considered at low magnetic field strengths. In this work we present a low field (LF) NMR signal diffraction based monitoring technique aimed at rapid non-invasive in-situ monitoring of hollow fiber membrane fouling (Sen et al., 1995; Lustig et al., 2007). To demonstrate this we monitor NMR diffraction during a fouling-cleaning cycle for a multi-fiber membrane module, where the foulant is alginate and cleaning agent is a sodium hydroxide solution (pH = 11). Fibers experiencing increased hydraulic resistance, due to fouling, cause flow re-distribution to non-fouled fibers. The resulting increase in heterogeneity is observed though the change of the measured nearest neighbour coherence pattern. We show that this effect is captured non-invasively by monitoring both the NMR Patterson function and power spectrum at different stages of fouling. This demonstrates that both the extent and structure of membrane module fouling can be determined rapidly using LF NMR (Yan, 2021; Fridjonsson et al., 2015). An ability which may be translated in future to improved cleaning protocols within the membrane industry.

2. Relevant background theory

An MRI is reconstructed via Fourier transform of the magnetic resonance signal acquired in **k**-space (Callaghan, 1993):

$$\rho(\mathbf{r}) = \int S(\mathbf{k})\exp[-i2\pi\mathbf{k} \bullet \mathbf{r}]d\mathbf{k} \tag{1}$$

where $\rho(\mathbf{r})$ is the spin density (Callaghan, 1993) at location **r**; $S(\mathbf{k})$ is the signal and $\mathbf{k} = \frac{\gamma \mathbf{G} t}{2\pi}$, where **G** is the applied magnetic field gradients, γ is the gyromagnetic ratio and t is the duration of applied gradient. The Wiener-Khinchin theorem (Cohen, 1998) relates correlation functions of one Fourier domain to the square of their transform in the other. Applied here the density autocorrelation function ($\phi(\Delta\mathbf{r})$) is given by the Fourier transform of the square of the imaging data, where V is the sample volume (Barrall et al., 1992):

$$\phi(\Delta\mathbf{r}) = \frac{1}{(2\pi)^3 V} \int |S(\mathbf{k})|^2 \exp(-i2\pi\mathbf{k} \bullet \mathbf{r})d\mathbf{k} \tag{2}$$

Equation (2) allows extraction of statistical information from the original imaging data in a manner analogous to conventional scattering experiments (Callaghan et al., 1991; Chen et al., 2012). The phase-suppressed imaging data, the power spectrum, $|S(\mathbf{k})|^2$ can be plotted with diffraction pattern rings indicating underlying regularity in structure. While the Fourier transform of the diffraction-data $|S(\mathbf{k})|^2$, i.e. the NMR Patterson function (**Eqn** (2), can be used to detail structure-length scale statistics. In the case of a system consisting of coherent structures, such as the hollow fiber bundles studied in this work, the NMR Patterson function will capture the structure coherence and the average nearest-neighbour distance, whilst the integral of $|S(\mathbf{k})|^2$ captures changes in fouling/cleaning state of the membrane module. This is because fiber fouling reduces signal coherence causing reduced intensity of signal diffraction peaks, conversely cleaning recovers the diffraction peak signal. In this work the use of a flow encoding magnetic field gradient is used to enhance contrast between fluid in fouled and non-fouled channels (Callaghan, 1993).

3. Materials and Methods:

The polyethersulfone (PES) ultrafiltration (UF) hollow fiber membrane module used in this study is a laboratory scale Microza SP series ultrafiltration module (SIP-1023) developed by Asahi Kasei corporation. Inside its 36 mm inner diameter (ID) housing, it has 401 closely packed straight hollow fibers as specified with an ID of 0.8 mm, fiber length of 205 mm with a membrane area of 0.2 m^2. The UF membrane has a molecular weight cut-off (MWCO) of 6 kDa. A schematic diagram of the flow loop used is shown in Fig. 1(a) with membrane module shown in Fig. 1(b). For the current experimental protocol, the permeate channel is shut after the extra-capillary space is filled with permeate, this is to allow for sensitive detection of any changes in ΔP at 0.1 kPa sensitivity as the system experiences early fouling.

An Oxford MARAN DRX NMR Rock Core Analyser (RCA), as shown in Fig. 1(c), employing a 0.3 T permanent magnet with a ^{1}H resonance frequency of 12.9 MHz was used to conduct the measurements. The RCA system has an inner bore diameter 53 mm, sufficient to accommodate the module (see Fig. 1(c)), and features 3D magnetic field gradients for spatial encoding thus enabling the performance of 2D imaging and velocity mapping across of transverse plane along vertical (Y) axis in these measurements. The maximum gradient strengths (T/m) are 0.27, 0.26 and 0.33 in the X, Y and Z direction respectively.

3.1. Experimental procedures

Deionized water was used as the flowing medium. A commercial sodium alginate powder (FMC Manugel GMB, MW = 170–230 kDa) was used to prepare the alginate solution at a concentration of 2,000 mg/L, CaCl$_2$ (LabServ) and NaCl (Analytical Reagent) were added at a concentration of 700 mg/l and 1,000 mg/l respectively to form alginate–calcium bonding, with Na$^+$ as the bonding-initiator (Yan, 2021). The resultant 0.2 wt% calcium-alginate solution was used as the foulant in all experiments performed. The foulant stock solution was diluted to 20 ppm in the feed-solution for the membrane element. Sodium hydroxide pellets (Analytical Reagent) was dissolved in deionized water to prepare the membrane cleaning solution with pH 11. The details of the flow loop used has been previously reported by Yan et al. (Yan, 2021). The total volumetric flow rate Q$_{total}$ was set at 100 mL min^{-1} for all imaging measurements.

The NMR experimental procedure performed was as follows using same fouling and cleaning procedure as reported in (Yan et al., 2023): seven consecutive MRI images were acquired. First MRI image (Image 1) was acquired for a clean module, then a dose of 20 ppm alginate solution was added 30 min before an MRI image (Image 2) was acquired. Another 20 ppm dose was added and 30 min later MRI image (Image 3) was acquired. Then four doses of 1 L of the pH 11 NaOH solution were sequentially added to the flow loop with each dosing taking 10 min. MRI image (Image 4) was acquired after 30 min of flowing at 100 mL min^{-1} (no soak case), Image 5 was acquired 30 min after allowing NaOH solution to soak module for 20 min. Image 6 was acquired 30 min after soaking module in NaOH solution for 1 h, and Image 7 was acquired after soaking module in NaOH solution for 10 h. Total experimental time was 24 h. Concurrently, single line of **k**-space (G$_{phase}$ = 0) was acquired. The full procedure of fouling and cleaning was performed twice for membrane module to test reproducibility of results. NaOH solution soaking was used in the current study to effectively minimise chemical usage, as flow channelling occurs during flash cleaning whereby NaOH solution preferentially travels through un-fouled fibers.

3.2. Imaging protocol

A spin echo imaging pulse sequence (Callaghan, 1993) using a Cartesian **k**-space raster was used with the MRI image plane set in the perpendicular-to-flow direction at distance of 40 mm from the fibers' entrance manifold. 2D MRI images were acquired with a field-of-view (FOV) of 75 mm by 75 mm with 512 by 512 voxels (phase direction was 152 zero-filled to 512) in the transverse plane resulting in an in-plane resolution of 146 μm and a slice thickness of 30 mm. To produce sufficient flow contrast the flow direction gradient strength was set
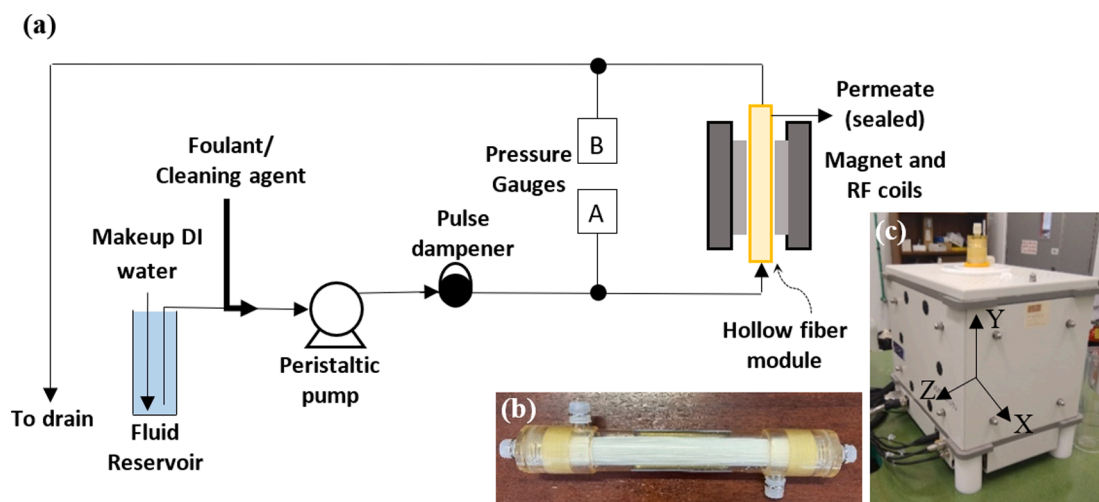
Fig. 1. (a) Schematic of the piping and instrumentation used for MRI velocity imaging experiments. The foulant or cleaning agent solutions were dosed into the system at the same inlet as the DI water upstream of the peristaltic pump. (b) Image of hollow fiber membrane module and (c) the low field benchtop MRI instrument with hollow fiber membrane module placed inside the magnet bore, with B_0 in the positive Z-axis direction in the transverse plane. Reproduced from Yan et al. (Yan et al., 2023).

at 0.8 Gauss/cm, with $\delta = 2$ ms and an echo time (T_E) of 38 ms. This flow contrasting accentuates the NMR signal attenuation due to flow inside the channels resulting in enhanced signal difference between fast flowing channels and channels experiencing a decrease in flow due to fouling. The number of scans was set at four as a four step phase cycle was used. Using a repetition time of 4 s the total acquisition time for each MRI was 42 min. For the single line **k**-space acquisition, with sweep width of 100 kHz, to obtain a coherence peak rapidly, the total
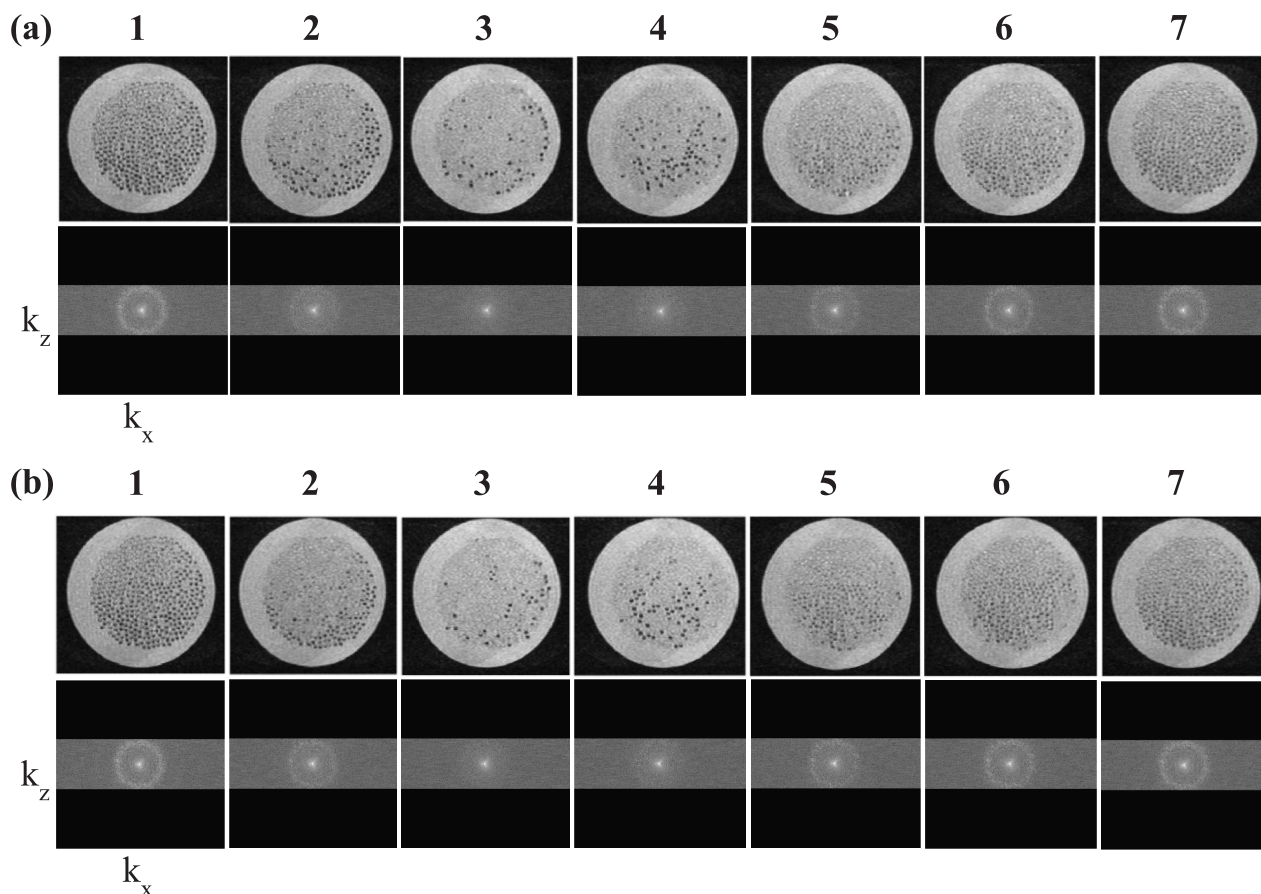
Fig. 2. MRI images (top row) and **k**-space images (bottom row) with flow encoding gradient obtained during the fouling/cleaning cycle of a membrane module – (a) Experiment 1 and (b) Experiment 2. **k**-space plot is plotted using absolute values on log10 scale, while the MRIs show membrane region (see supplementary material for full MRIs) – this is to better visualise the **k**-space coherence ring structure, and ease visual comparison with the membrane region in MRIs as the coherence ring structure disappears and re-appears while system is fouled (1–3) and cleaned (4–7). The x and z represent read encode direction and phase encode direction respectively. The images are acquired 40 mm from the fiber's entrance manifold.

acquisition time was 16 s. Velocity imaging protocol used for the experiments as outlined in detail in Bin et al. (Yan et al., 2023), and these were performed at the same time as the reduced **k**-space MRI images were acquired.

4. Results and discussion

4.1. MRIs and k-space

Fig. 2 shows MRIs obtained whilst the hollow fiber membrane module was fouled twice using alginate (2, 3) followed by cleaning using NaOH solution (pH = 11), first by flash cleaning (4) then followed by soaking for 0.33 h, 1 h and 10 h (5, 6 and 7). Below each image is the corresponding **k**-space with the ring-like coherence feature visible. This experiment was repeated to produce the second set of measurements (Fig. 2b). Below each set of MRIs is the reduced **k**-space, in phase direction (k_z), where the coherence feature (ring-structure) is observed to disappear and reappear during the experiment going from MRI 1 to 7.

4.2. Model vs. Experiments: Diffraction

To assess the effect of signal change inside the membrane module fibers on the resultant **k**-space coherence feature a model was produced consisting of a discretised matrix (512 by 512) with the fiber bundle generated using the masked fiber bundle obtained from MRI (1) of the hollow fiber (HF) membrane module. In the model MRI voxels inside each fiber and voxels outside the module were set to zero, while voxels outside the fibers but inside module were set to one (see Fig. 3a). Fig. 3b shows the resultant NMR Patterson function produced using Eqn. (2) with the water filled modules size and circular shape captured by the main signal attenuation. Fig. 3c shows the zoomed in view of the centre of Fig. 3b which shows the diffraction pattern due to nearest neighbours produced by fibers. This corresponds to distance of ~ 1.2 mm, which is on the order of the outer diameter of the closely packed fibers.

To model the effect of random stagnation of flow in the fiber, flowing fibers were switched off by simulating them as contributing the same total signal as an equivalent volume of stagnant fluid when they were 'fouled' (all voxels changing from zeros to ones). This was done in increments of 50 randomly chosen fibers until all fibers were 'fouled'. While the model does not contain the intricacies of the actual system such as partial voxel signal contributions and noise, the fidelity of the model to the actual system is indicative of the relative importance of these features. Using this simple model, it is possible to systematically 'foul' fibers (voxels transition from zeros to ones inside fibers) to calculate the effect this has on the nearest neighbour diffraction pattern in the respective Patterson function.
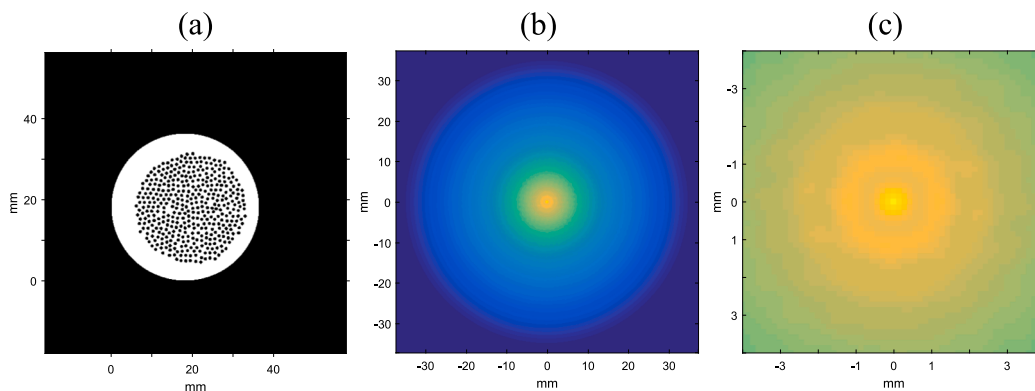
4.3. NMR Patterson functions

When the NMR Patterson functions for the model results are analysed (see Fig. 4) it can be observed that for the clean image (Fig. 4a) there is a nearest neighbour diffraction pattern. Modelling random fouling of fibers, shown here using an increment of one hundred fibers, a gradual change in diffraction pattern is observed with increasing loss of nearest neighbour diffraction peaks. Fig. 4f shows the radial integral of the NMR Patterson function, showing nine curves at 50 fouled fiber increment (0 to 401 fouled fibers). Insert image is zoomed into the 0–4 mm length scale. A nearest neighbour diffraction peak at ~ 1.2 mm is observed corresponding well to the size of the tightly packed hollow fibers (outer diameter: 1.2 mm).

Fig. 5 shows the radial integral of the Patterson functions acquired during the fouling/cleaning cycle of a membrane module for experiment 1 and 2 respectively. Both experiments show the same pattern with the coherence peak associated with nearest neighbours (~1.2 mm) largely disappears during the course of fouling (Test 1 to Test 3), but then re-emerges during the cleaning process (Test 4 to Test 7). The ineffectiveness of flash cleaning during the current study (Test 4) is evident in the results, while the soaking of the module for extended periods of time (Test 5 to Test 7) eventually recovers the coherence feature, although it is now less prominent due to the presence of residually fouled fibers (Yan et al., 2023).

The observed diffraction peaks are observed to be sensitive towards apparent residual fouling (Yan et al., 2023) of the module as the before fouling (Test 1) and after cleaning (Test 7) show similar diffraction peaks, but the intensity of the diffraction peaks is diminished. This observed sensitivity to residual fouling is of particular interest for early fouling warning. A further impetus for this mode of fouling monitoring is that it offers a rapid NMR based monitoring technique as only limited frequencies of **k**-space corresponding to the length-scale of coherence feature (Barrall et al., 1992) need to be monitored.

4.4. Correlation of diffraction peak intensity and number of fouled fibers

Fig. 6a shows the evolution of $|S(\mathbf{k})|^2$ generated using the model as an increasing number of fibers are fouled which shows a systematic decrease in the coherence peak. This allows comparison with the results from the fouling/cleaning experiments (Fig. 6b and Fig. 6c) which shows a similar location of the coherence peak (~1 mm^{-1}) whilst an observed decrease in the coherence peak can be directly compared by to the number of flow active fibers (Yan et al., 2023) during Test 1 to Test 7. A pattern emerges in the experimental data where the loss of fibers causes the diffraction peak to diminish in intensity until it is only weakly evident during Test 3, after two doses of foulant have been added. The coherence peak gradually recovers during the subsequent cleaning (Test 4 to Test 7). It is notable that the peak is less intense in Test 7 than Test 1,

Fig. 3. Shows (a) model MRI image (binary values), (b) NMR Patterson function, (c) zoom-in plot of (b). The nearest neighbour ring seen in the Patterson function is at ~ 1.2 mm (consistent with the outer diameter of the closely packed fibers).
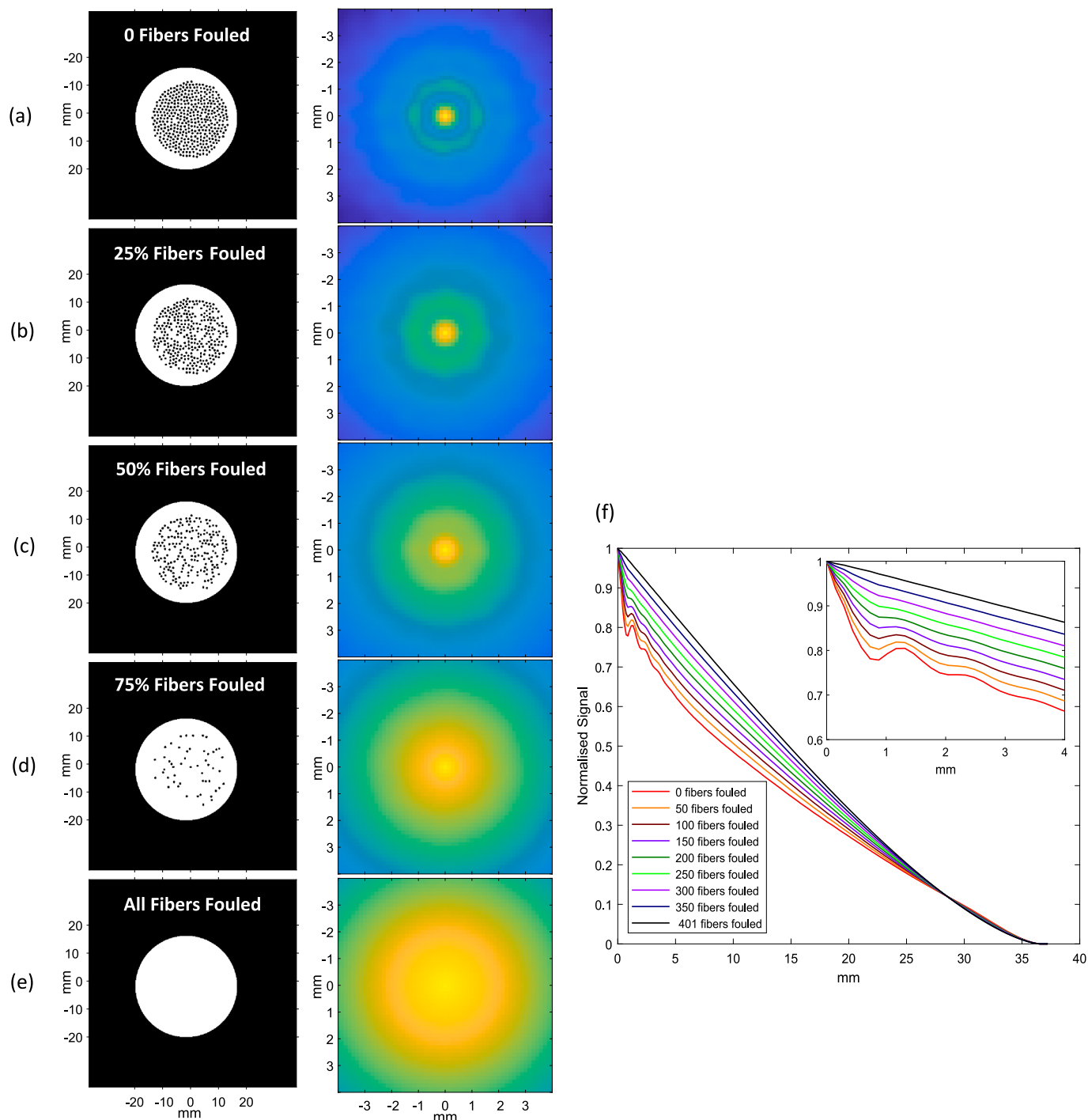
Fig. 4. Simulated MRI module images (left) and Patterson functions (right) for (a) to (e): 0, 100, 200, 300 and 401 fouled fibers. The nearest neighbour diffraction pattern seen in (a) disappears as more fibers are fouled. (f) shows the radial integral of the full Patterson function (0–40 mm), averaged over 50 model runs, with the insert image showing the central region of the Patterson function (0–4 mm). See S1 in supplementary material for model MRI and Patterson functions for all nine fouling cases modelled (from 0 to 401 fibers fouled in increments of 50 fibers).

indicating that there is a residual fouling effect in the module even after 10 h of NaOH soaking. It is also important to note that the results are highly reproducible between experiment 1 and 2.

4.4.1. Rapid detection of signal coherence loss (single line k-space detection)

To assess whether these diffraction patterns (Fig. 6) are able to quantify the percentage (%) fibers fouled, velocity images obtained from experiment 1 and 2 were assessed using approach presented in Bin et al.

(Yan et al., 2023) to obtain the percentage (%) of fibers which are assessed fouled in this work if a fiber has its volumetric flow (Q_{fiber}) reduced by greater than 5% from the initial non-fouled flow (i.e. Test 1). This allows for better comparison with the binary model data results. Fig. 7 shows a plot of the signal attenuation against % fouled fibers, with signal obtained from the first coherence peak using only the centreline of **k**-space (Fig, 7). The signal shown is the full width at half maximum (FWHM) peak signal, divided by the initial FWHM peak signal before fouling/cleaning cycle commences. For the modelled data results a

(a)

(b)
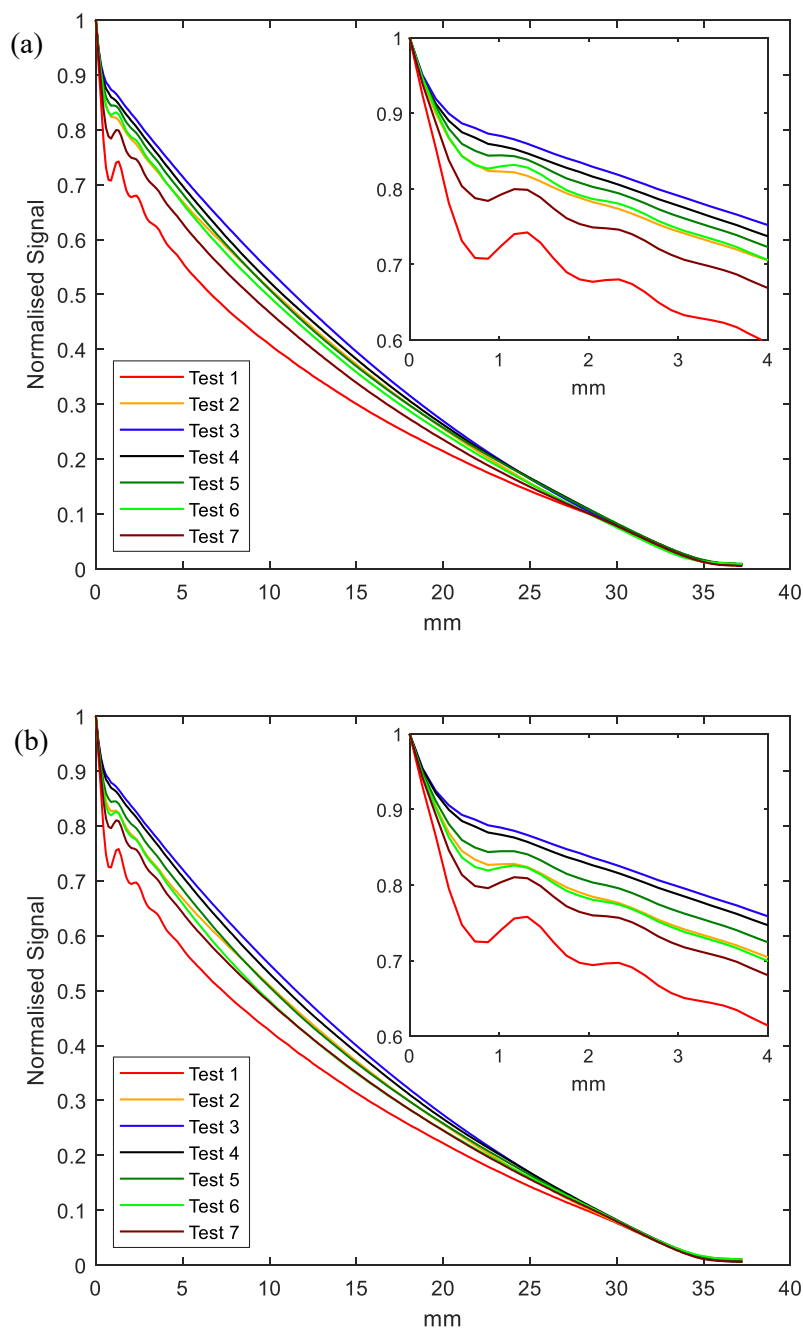
Fig. 5. Shows plots of the radial integral of the Patterson functions obtained during the fouling/cleaning cycle of a membrane module – (a) Experiment 1 and (b) Experiment 2. See S2 and S3 in supplementary material for MRI and Patterson functions for all seven tests. Insert plots show the initial 4 mm length scale to better show the coherence peaks in the data. A minimum is seen at ~ 0.9 mm. Corresponding to the nearest neighbour's coherence structure. As fouling progresses (Test 1 to Test 3) there is a loss in diffraction peak, while during progressive cleaning (Test 4 to Test 7) there is a re-emergence of the coherence peak, however due to residual fouling it does not return to its original shape.

Monte Carlo simulation was run with n = 50 runs at each increment and the average result is plotted.

A strong correlation is observed between the signal and number of fouled fibers consistent with expectations based on the NMR Patterson function results (see section 4.3). It is observed that the experimental data is scattered and skews slightly towards smaller values than the model, which may be partly due to the binary nature of the model, and due to the real system experiencing a range of fouling and membrane signal effects within the fibers at each fouling/cleaning stage which modulate the fiber signal (Yan et al., 2023) and may deviate from random fiber fouling due to non-random fouling structure effects. However, importantly the results show that there is a strong correlation between the number of fouled fibers and signal, and that this is reasonably well captured by a random fouled fiber model. This demonstrates the possibility of measuring only the coherence feature signal to monitor the extent of fouling inside the membrane module. This type

of information could then be directly communicated to an operator when monitoring fouling extent and cleaning efficiency.

Further refinement of the assessment of fouled fibers may improve the accuracy of this technique, as the current assessment of fouling is dependent on the reduction in flow compared with initial volumetric flow within a fiber. This can also be an indicator of change in flow field upstream of membrane module due to fouling which causes a measurable redistribution of flow through the channels. This is an area of particular interest for further study as the determination of sensitivity of the technique to early and residual fouling due to the observation of large signal attenuation measured at relatively modest changes in the flow field (i.e. Test 1 and Test 7). It is important in this respect to note that based on pressure measurements performed (Yan et al., 2023) (i.e. feed channel pressure drop (FCP) measurement at 0.1 kPa sensitivity) Test 1 and Test 7 are indistinguishable for both Experiment 1 and 2.

A fundamental reason for the high sensitivity of this monitoring
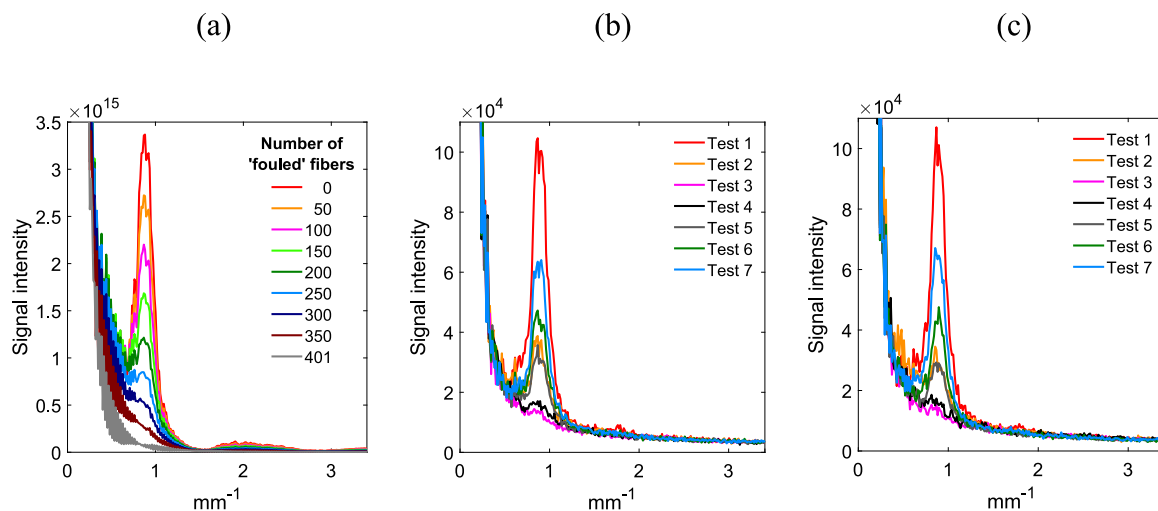
Fig. 6. (a) Model result for the radial integration of $|S(k)|^2$ function as the number of 'fouled' fibers increases – with the location of fibers determined randomly. (b) and (c) Experimental $|S(k)|^2$ results for the 1st and 2nd experimental fouling/cleaning cycles. The coherence feature largely disappears at the 2nd fouling (Test 3) and 1st cleaning (Test 4) stage – indicative of ineffective cleaning – whilst subsequent cleaning results in the gradual recovery of the feature (Test 5 to Test 7). It is notable that the feature is quite a bit lower in Test 7 than Test 1, indicating that there is residual fouling in the module even after 10 h or NaOH soaking.
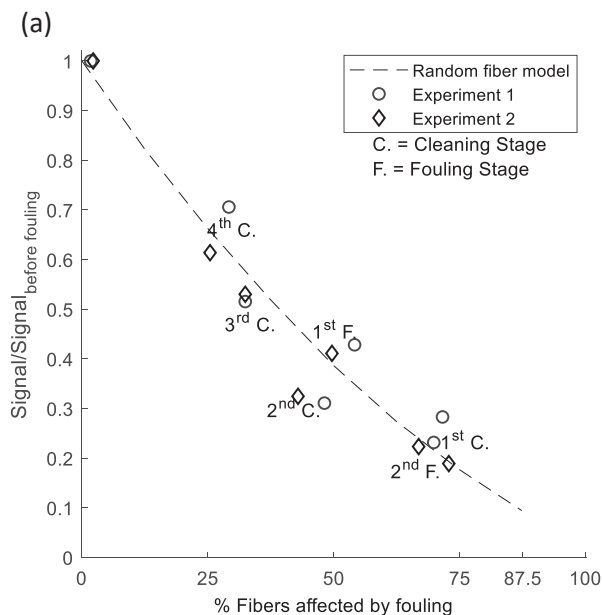
Fig. 7. Shows the correlation between the signal obtained for the $|S(k)|^2$ coherence peak from the centre-line of k-space plotted against the % of fibers with greater than 5% reduction in volumetric flow which is fibers assessed from velocity images (see (Yan et al., 2023) for reference). For comparison the same correlation for the Monte Carlo model (n = 50) is shown for random fiber fouling (black dash line). It can be seen that there is a strong correlation between % fibers affected by fouling and the magnitude of the coherence peak. Experiment 1 & 2 are detailed in Section 3.1; They consist of two experimental runs, where in each run the module experiences two doses of alginate fouling (1st and 2nd fouling stage) followed by four cleaning stages using pH = 11 NaOH solution (1st C: flash cleaning; 2nd C: 20 min soak cleaning; 3rd C: 1 h soak cleaning and 4th C:10 h soak cleaning).

technique is because very small changes in hydrodynamic resistance can divert flow in a parallel fiber membrane module. These observations of the monitoring technique's sensitivity, which combined with rapid detection (on order of seconds), opens the potential for very early warning of flow changes within a multifiber hollow fiber membrane module or similar parallel flow systems suitable to NMR monitoring. Further research is ongoing to improve the modelling of the system with a focus on both different fouling structures (e.g. random voxel fouling), signal attenuation (e.g. non-binary model of fouling) and influence of SNR contributions on the modelling, to determine the influence of these factors on the resultant diffraction signal monitoring.

The current research using the technique presented in this research will be in the future extended to permeate fluxing HF membrane modules containing 100s to 1000s of fibers with an aim to correlate the local NMR diffraction measurement presented here with more traditional permeate flux monitoring. This will allow examination of the local structural correlation features measured with the technique presented, such that the sensitivity of the localised observation of the effect of permeation can be correlated to the measured bulk permeation to quantify sensitivity to localised fouling.

5. Conclusions

Early and rapid detection of fouling of hollow fibers is demonstrated in this study. In this research we have obtained NMR Patterson functions during a fouling/cleaning cycle for a multi-fiber hollow fiber system. The nearest neighbour diffraction peaks were observed to disappear and re-appear as the module was fouled using sodium alginate and subsequently cleaned using NaOH solution (pH = 11). The nearest neighbour distance measured (~1.2 mm) was consist with the outer diameter (1.2 mm) of the hollow fibers in the tightly packed fiber bundle. Monte Carlo modelling of fouling as a binary effect on fibers corresponded well with the measured data from the fouling measurements. Using the power spectrum ($|k|^2$) data and integrating over the full width at half maximum (FWHM) peak of the first coherence peak a strong correlation was obtained between the signal attenuation and the number of fibers affected by fouling. This shows that it is possible to monitor a single line of k-space to monitor the fouling state of the module, therefore not necessitating full k-space imaging. This allows a rapid modality of fouling monitoring of multi-fiber systems. The approach demonstrated in this work for a fouling/cleaning cycle for a hollow fiber membrane module may be translatable to systems which exhibit similar strong structural coherence and resultant diffraction peaks, where a flow encoding gradient can be applied to suppress signal from a flowing fluid component, and may be used for complex flow system if the relevant length scale of interest is separable (different) from other length scales in the

system.

Declaration of Competing Interest

The authors declare that they have no known competing financial interests or personal relationships that could have appeared to influence the work reported in this paper.

Data availability

Data will be made available on request.

Acknowledgments

Appendix A. Supplementary data

Supplementary data to this article can be found online at https://doi.org/10.1016/j.ces.2023.118925.

References

Albers, P.W., Parker, S.F., 2021. Applications of neutron scattering in technical catalysis: characterisation of hydrogenous species on/in unsupported and supported palladium. Top. Catal. 64 (9), 603–613.

Barrall, G.A., Frydman, L., Chingas, G.C., 1992. NMR diffraction and spatial statistics of stationary systems. Science 255 (5045), 714–717.

Callaghan, P.T., 1993. Principles of nuclear magnetic resonance microscopy. Oxford University Press on Demand.

Callaghan, P.T., Coy, A., MacGowan, D., Packer, K.J., Zelaya, F.O., 1991. Diffraction-like effects in NMR diffusion studies of fluids in porous solids. Nature 351 (6326), 467–469.

Callaghan, P.T., Codd, S.L., Seymour, J.D., 1999. Spatial coherence phenomena arising from translational spin motion in gradient spin echo experiments. Concepts in Magnetic Resonance 11 (4), 181–202.

Chen, S.H., B. Chu, and R. Nossal, *Scattering techniques applied to supramolecular and nonequilibrium systems*. Vol. 73. 2012: Springer Science & Business Media.

Cohen, L. The generalization of the wiener-khinchin theorem. in 1998 IEEE International Conference on Acoustics, Speech and Signal Processing, ICASSP'98 (Cat. No. 98CH36181). 1998. IEEE.

Fridjonsson, E.O., Creber, S.A., Vrouwenvelder, J.S., Johns, M.L., 2015. Magnetic resonance signal moment determination using the Earth's magnetic field. J. Magn. Reson. 252, 145–150.

Gebel, G., Diat, O., 2005. Neutron and X-ray scattering: suitable tools for studying ionomer membranes. Fuel Cells 5 (2), 261–276.

Grunwaldt, J.-D., Schroer, C.G., 2010. Hard and soft X-ray microscopy and tomography in catalysis: bridging the different time and length scales. Chem. Soc. Rev. 39 (12), 4741–4753.

Hoult, D.I. and R.E. Richards, *The signal-to-noise ratio of the nuclear magnetic resonance experiment.* Journal of Magnetic Resonance (1969), 1976. **24**(1): p. 71-85.

Li, X., Mo, Y., Li, J., Guo, W., Ngo, H.H., 2017. In-situ monitoring techniques for membrane fouling and local filtration characteristics in hollow fiber membrane processes: a critical review. J. Membr. Sci. 528, 187–200.

Lustig, M., Donoho, D., Pauly, J.M., 2007. Sparse MRI: The application of compressed sensing for rapid MR imaging. Magnetic Resonance in Medicine: An Official Journal of the International Society for Magnetic Resonance in Medicine 58 (6), 1182–1195.

Mansfield, P., Grannell, P.K., 1973. NMR'diffraction'in solids? J. Phys. C Solid State Phys. 6 (22), L422–L426.

Mansfield, P., Grannell, P.K., 1975. " Diffraction" and microscopy in solids and liquids by NMR. Phys. Rev. B 12 (9), 3618–3634.

Marchesini, S., He, H., Chapman, H.N., Hau-Riege, S.P., Noy, A., Howells, M.R., Weierstall, U., Spence, J.C.H., 2003. X-ray image reconstruction from a diffraction pattern alone. Phys. Rev. B 68 (14), 140101.

Saad, M.A., 2004. Early discovery of RO membrane fouling and real-time monitoring of plant performance for optimizing cost of water. Desalination 165, 183–191.

Schuhmann, S., Schork, N., Beller, K., Nirschl, H., Oerther, T., Guthausen, G., 2018. In-situ characterization of deposits in ceramic hollow fiber membranes by compressed sensing RARE-MRI. AIChE J 64 (11), 4039–4046.

Sen, P.N., Hürlimann, M.D., de Swiet, T.M., 1995. Debye-Porod law of diffraction for diffusion in porous media. Phys. Rev. B 51 (1), 601–604.

Seymour, J.D., Callaghan, P.T., 1997. Generalized approach to NMR analysis of flow and dispersion in porous media. AIChE J 43 (8), 2096–2111.

Shemesh, N., 2020. Measuring Microstructural Features Using Diffusion MRI. Advances in Magnetic Resonance Technology and Applications 1, 571–604.

Sim, L.N., Chong, T.H., Taheri, A.H., Sim, S.T.V., Lai, L.i., Krantz, W.B., Fane, A.G., 2018. A review of fouling indices and monitoring techniques for reverse osmosis. Desalination 434, 169–188.

Song, Y.-Q., Ryu, S., Sen, P.N., 2000. Determining multiple length scales in rocks. Nature 406 (6792), 178–181.

Tanner, B.K., *X-ray diffraction topography: international series in the science of the solid state.* Vol. 10. 2013: Elsevier.

Vrouwenvelder, J.S., Van Loosdrecht, M.C.M., Kruithof, J.C., 2011. Early warning of biofouling in spiral wound nanofiltration and reverse osmosis membranes. Desalination 265 (1–3), 206–212.

Vrouwenvelder, J., Vanpaassen, J., Wessels, L., Vandam, A., Bakker, S., 2006. The membrane fouling simulator: a practical tool for fouling prediction and control. J. Membr. Sci. 281 (1-2), 316–324.

Warren, B.E., *X-ray Diffraction.* 1990: Courier Corporation.

Yan, B., et al., 2021. Monitoring of hollow fiber module velocity field and fouling inside individual fibers using benchtop MRI. J. Membr. Sci. 629, 119238.

Yan, B., Blankert, B., Vogt, S.J., Vrouwenvelder, J.S., Johns, M.L., Fridjonsson, E.O., 2023. Monitoring residual fouling after cleaning of multi-fiber membrane modules fiber-by-fiber using non-invasive MRI monitoring. Water Res. 229, 119384.